Available online at www.sciencedirect.com
ScienceDirect
Ceramics International 38 (2012) 29–38
CERAMICS INTERNATIONAL
www.elsevier.com/locate/ceramint

Microstructural and electrical characterization of bulk $YBa_2Cu_3O_{7-\delta}$ ceramics

S. Suasmoro [a,1], M.F. Khalfi [b], A. Khalfi [b,*], G. Trolliard [c,1], D.S. Smith [a,1], J.P. Bonnet [a,1]

[a] Groupe d'Etude des Matériaux Hétérogènes, Centre Européen de la Céramique, 12, rue Atlantis, 87068 LIMOGES Cedex, France
[b] Laboratoire de Matériaux et Systèmes Réactifs, B. P. 89, Avenue Larbi BEN M'HIDI, University Djillali LIABES – Sidi Bel Abbès, 22000 Sidi Bel Abbes, Algeria
[c] Sciences des Procédés Céramiques et Traitements de Surface, Centre Européen de la Céramique, 12, rue Atlantis, 87068 LIMOGES Cedex, France

Received 1 June 2009; received in revised form 14 March 2011; accepted 2 April 2011
Available online 31st May 2011

Abstract

The value of critical current density at 77 K in ''zero'' applied field (J_c) characterizing the superconducting state for $YBa_2Cu_3O_{7-\delta}$ ceramics is closely related to the microstructure.

The interrelationships between the microstructural factors such as pore volume fraction, oxygen content, average grain size, are complex. However, these factors also influence the normal state resistivity measured at room temperature (ρ_{300}). We demonstrate how the current carrying cross section influences *Jc* and ρ_{300} in a similar way. Data, reported for two classes of $YBa_2Cu_3O_{7-\delta}$: small grain porous ceramics and larger-grain denser ceramics, reveal an approximate linear relation between $\rho_{300\,K}$ and J_c. Extrapolation of this relation to a fully dense small grain $YBa_2Cu_3O_{7-\delta}$ ceramic yields values of $\rho_{300} = 0.4$ mΩ cm and $J_c = 10^3$ A cm^{-2}.

Keywords: Superconductor; $YBa_2Cu_3O_{7-\delta}$ Synthesis; A. Sintering; Porous ceramic-limited grain growth; Conductivity; Microcracks; Critical; Current; Magnetic; Field

1. Introduction

Since 1987 ceramic oxides have been formulated, which exhibit superconductivity at a temperature above that of liquid nitrogen [1]. This has opened up the possibility of high current applications for these materials in systems using less expensive cryogenics. However one of the restraining aspects in such a development has been a relatively low value of transport critical current density (J_c) measured for $YBa_2Cu_3O_{7-\delta}$ (and its derivatives) when it is prepared in a bulk ceramic form. The value of (J_c) at 77 K usually does not exceed 10^3 A cm^{-2} in non-textured polycrystalline ceramics [2–4] while melt textured growth material has exhibited values above 10^4 A cm^{-2} [5,6] and thin films have achieved a value close to 10^6 A cm^{-2} [7–9]. It is therefore important to understand the factors which control the electrical response. The aim of the present paper is to examine in some detail the influence of microstructural variation on the normal and superconducting transport behavior of polycrystalline $YBa_2Cu_3O_{7-\delta}$. It will be shown for certain parameters that there is a close relation between their effect on both normal and superconducting states.

Many factors have been cited to explain variation in critical current: alignment of grains, grain boundaries, oxygen content, residual carbonates [10–12], porosity, microcracks and sample geometry [13–15]. In earlier works careful attention was paid to elimination of CO_2 during calcination of attrition milled mixture of Y_2O_3, CuO, and $BaCO_3$ [16]. After calcination of the powder, samples were pressed and sintered without delay in order to avoid degradation, which occurs in a moist atmosphere. An alternative approach [17] has been developed where degraded powder of an industrial origin was restored to its original state by thermal treatment just below the temperature at which liquid forms in the Y_2BaCuO_5–$BaCuO_2$–CuO_x system. Samples of this type were also prepared for comparison. As yet no relation between grain size (and, hence, the number of grain boundaries in the current path) and the transport critical current density has been reported except for the influence of grain growth-induced microcracking which is detrimental [18,19,20].

By a careful choice of sintering conditions above and below the appearance of a liquid phase at 925 °C in oxygen, controlled

* Corresponding author. Tel.: +213 0 770 60 03 47.
E-mail addresses: lmsr@univ-sba.dz (A. Khalfi), gemh.ensci@unilim.fr (G. Trolliard).
[1] Tel.: +33555452222.

0272-8842/$36.00 © 2011 Published by Elsevier Ltd and Techna Group S.r.l.
doi:10.1016/j.ceramint.2011.05.133

variation in the microstructure was achieved in terms of porosity, average grain size, presence of microcracks, and to a certain extent oxygen content. Electrical measurements at room temperature and in liquid nitrogen were then performed on samples of similar geometry.

The critical current densities (J_c) at 77 K and the normal state resistivity (ρ_{300}) are used to characterize the electrical properties of $YBa_2CuO_{7-\delta}$ ceramics. From the technological point of view the aim is to achieve the maximum possible value of J_c. This should be associated with a low value of ρ_{300} since the imperfections in the ceramic which limit J_c also yield additional resistance in the normal state. A simple model for the electrical response is proposed with respect to the relation of J_c to ρ_{300}.

2. Experimental

2.1. Sample preparation

Samples were prepared from two types of powder. Powder A was obtained by attrition milling with zircon beads of a stoichiometric mixture of Y_2O_3, $BaCO_3$, and CuO followed by the calcination of 5 g batches at 850 °C for 6 h in flowing air [21,22]. The purity of the starting powder was 99.99% or greater. A second milling step of 1 h was necessary to break agglomerates and gave a specific surface area of 1.7 $m^2\ g^{-1}$. X ray diffraction measurements of the calcination product showed traces of second phases, identified as CuO and $BaCuO_2$, which eliminated themselves during sintering. The powder was pressed uniaxially with 50 MPa into disk samples using a 13 mm die; giving green densities in the range from 45 to 50% of the theoretical value. The sintering behavior was characterized in a practical manner by isothermal dilatometric experiments. Corresponding to a typical cycle, the initial ramp to the dwell temperature was 3 °C per minute and the length change was measured using a differential dilatometer (Adamel Lhomargy DI-10). The evolution of the microstructure was also assessed with respect to grain growth. Scanning electron microscope observations were made on polished surfaces, which had been chemically etched in a dilute solution of HCl. Fig. 1 shows the SEM micrograph (A) for ceramic sintered under oxygen at 915 °C during 12 h and micrographs of samples corresponding to different sintering stages (oxygen

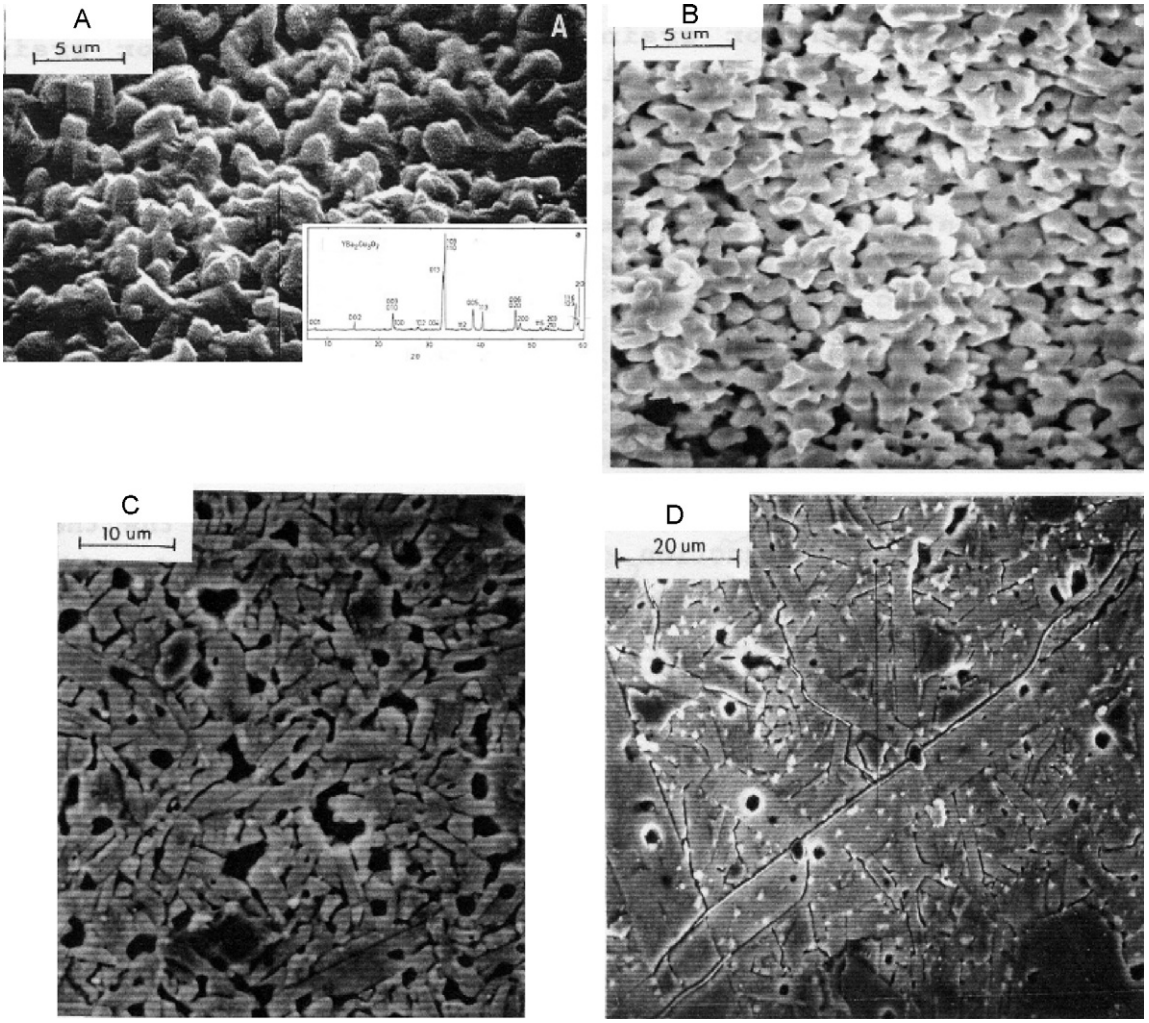

Fig. 1. (A) SEM micrograph for ceramic sintered under oxygen, at 915 °C during 12 h, (B) sample sintered at 925 °C for 6 min, (C) sample sintered at 950 °C for 36 min, (D) sample sintered at 955 °C for 360 min.

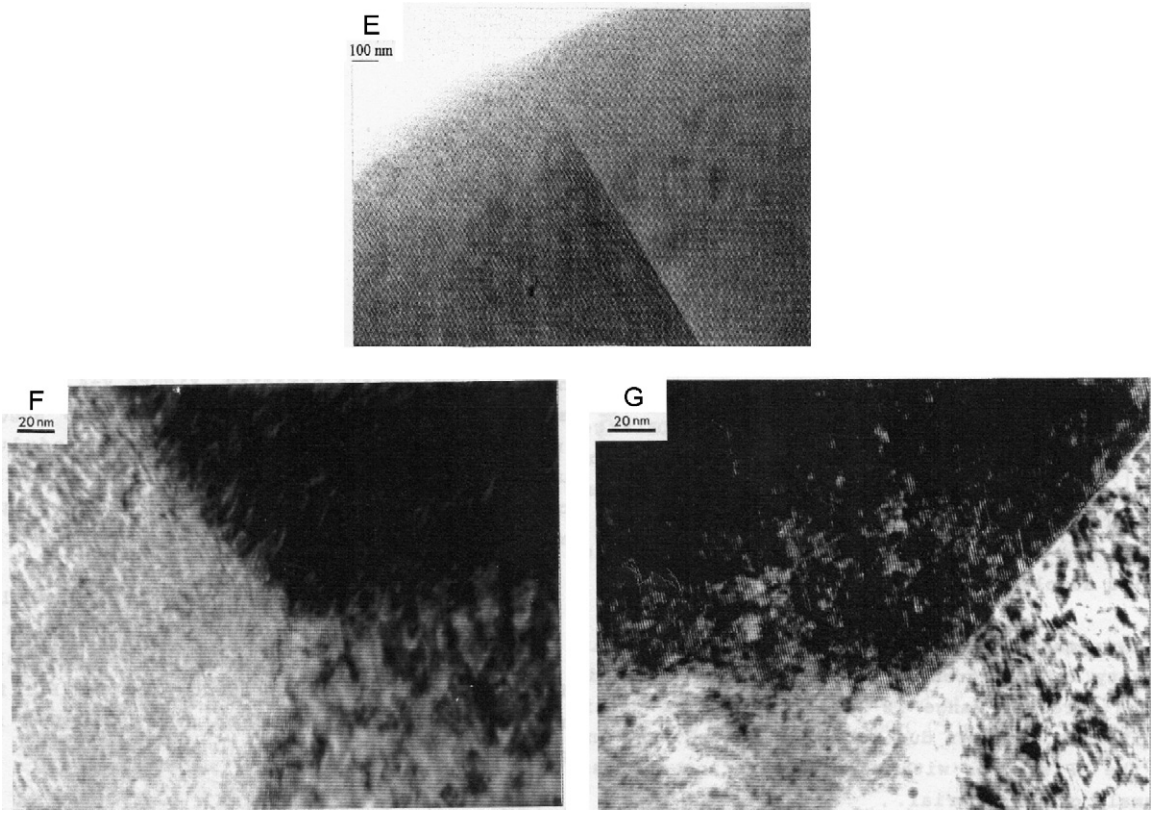

Fig. 2. (E) TEM observation of grain boundary for ceramic sintered under oxygen at 915 °C during 12 h, (F) TEM micrographs for sample sintered in oxygen at 915 for 48 h, (G) TEM micrographs for sample sintered in oxygen at 925 for 6 h.

atmosphere), 925 °C during 60 min (B), 950 °C during 36 min (C) and 950 °C during 360 min (D). Fig. 2 shows the TEM observations of grain boundaries for ceramic sintered under oxygen at 915 °C during 12 h (E), TEM micrographs for samples sintered in oxygen at 915 °C for 48 h (F) and 925 °C for 6 h (G). The grain boundaries and triple points seem clean. However occasionally an amorphous phase was found in the grain boundary, but further analysis did not indicate any difference with the matrix. For the sample sintered at 915 °C, the grain boundaries are clean without any ambiguity (Fig. 2F). The liquid phase present during sintering at 925 °C which has been observed by ultrasonic measurement [23], could therefore be perfectly recrystallized to $YBa_2Cu_3O_{7-\delta}$ during cooling.

Three temperatures were chosen, 900 °C, 925 °C and 950 °C characterizing the different domains obtained by dilatometric curves as a function of temperature in oxygen and in air for samples pressed from planetary milled powder and from attrition milled powder. The average grain size was determined by a linear intercept method. Further evidence is revealed by shrinkage during isothermal treatment in oxygen. The data are plotted in log–log form and shown in Fig. 3. The linear behavior for the sample held at 900 °C is very striking. Using the equation obtained by an empirical relation for the shrinkage dependence on time.

$$\frac{dL}{L_0} = kt^m, \tag{1}$$

where dL is the length change, L_0 is the initial sample length, and k is a constant. For solid state sintering the exponent m typically ranges from 1/3 to 1/2, consistent with the analysis of theoretical models. Fitting gives $m = 0.33$ with a correlation coefficient for linear regression $R^2 = 0.99$ which is in good agreement with the result reported by Chen et al. [24]. It suggests strongly that the densification at 900 °C is sufficiently slow meaning the duration of the dwell will determine the final density and that solid state sintering is predominant at this temperature. It can be noted there is no major evolution in the average grain size (less than 2 μm).

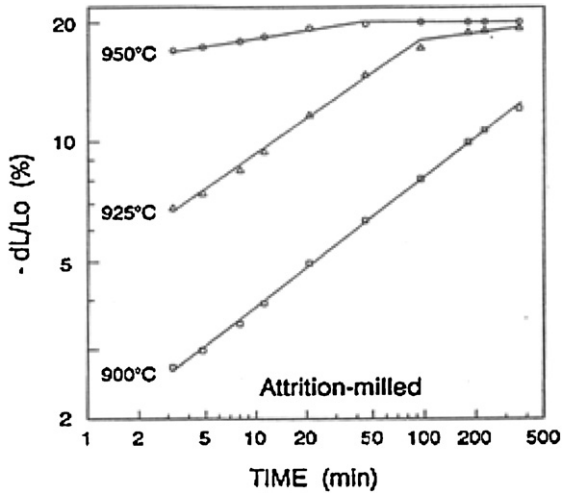

Fig. 3. Isothermal shrinkages at different temperatures in oxygen.

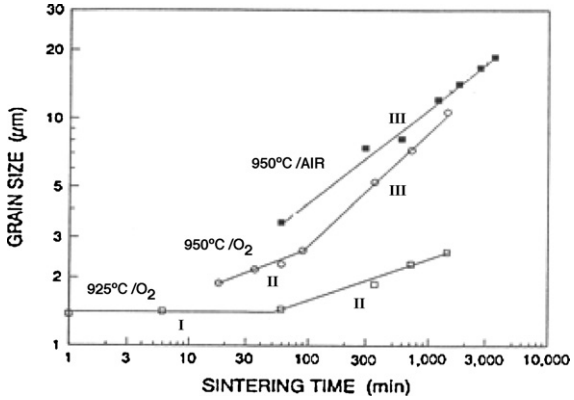

Fig. 4. Grain growth for different isothermal treatments for attrition milled powder. The stages are indicated.

By contrast at 950 °C the densification is virtually completed before the dwell starts. For $YBa_2Cu_3O_{7-\delta}$, using the Mendelson approach [25] to estimate the average grain size, the evolution of grain size was studied as a function of time at a given temperature and atmosphere. Fig. 4 indicates that grain growth will be significant for a firing cycle at 950 °C, providing strong evidence to support a liquid phase sintering mechanism above 925 °C. In conclusion two major classes of microstructures can be obtained depending on the firing temperature: an approximately constant small grain size less than 3 μm with a variable porosity, or an approximately constant porosity of 10% and a variable grain size. The final densities were evaluated using dry mass and volume measurements. A number of samples were checked by the technique based on Archimedes' principle.

Powder B was supplied by Rhône-Poulenc and was nonstoichiometric with a composition of $YBa_{1,98}Cu_{3,04}O_{7-\delta}$. The preparation via nitrates yielded a specific surface area of 2.4 $m^2\ g^{-1}$ and a thermal treatment, following the procedures in reference [18] prior to sintering, was used to restore the major phase after storage. By sintering at 915 °C for different periods, samples with average grain size less than 2 μm and variable porosity were obtained.

2.2. Electrical characterization

For electrical characterization samples were cut into thin bars, typically (10–11) mm long with a standard cross sectional area of 1 mm^2. The room temperature resistivity and the current–voltage behavior in liquid nitrogen at 77 K for «zero» magnetic field were measured using a 4 terminal configuration. «zero» field refers to Zero applied magnetic field but includes the presence of the earth's magnetic field of approximately 0.5×10^{-4} T. Two major problems present themselves in these measurements.

First it is necessary to achieve very small contact resistance between the copper connecting wires and the $YBa_2Cu_3O_{7-\delta}$ bar at the current terminals in order to minimize Joule heating at the end. For this a first layer of silver paste (series A: Biorad A 1208 quick dry colloidal, series B Démetron 200 silver paste) was painted on the ends and the sample was given a thermal treatment at 500 °C in oxygen. After wrapping the copper wire onto the contact pad, the electrical contact was completed with a quick dry colloidal silver yielding less then 0.1 Ω resistance for the two current terminals. In order to test the existence of heating effect, critical current measurement was carried out on a sample with a six point configuration Fig. 5A. The inner voltage terminals gave a critical current 5 A where as the outer voltage terminals gave a critical current of 4 A. This confirmed that the ends were significantly hotter than the middle part of the bar. Given a combined current electrode resistance of 1 Ω, this corresponds to approximately 25 W or 12.5 at each end. The description of heat transfer between ceramic and liquid nitrogen is not simple, but an interesting estimate can be made. For steady state heat transfer to the sample during (J_c) measurement (Fig. 5B) the heat generated by the contact resistance must be dissipated and can be denoted Q. A proportion flows to the 123 ceramic bar sample denoted Q'. The sample temperature T_s can be estimated by:

$$T_s = 77 + \frac{Q'}{hA}, \tag{2}$$

where h is heat transfer coefficient between the ceramic and liquid nitrogen liquid and A is surface area of the sample in contact with the liquid nitrogen. When liquid nitrogen boils and assuming that the temperature difference between the ceramic surface and liquid nitrogen is ~10 K, the heat transfer coefficient can be taken to be 1.5 kW m^{-2} K^{-1}. In the worst possible case where the condition above in fulfilled (for which the $YBa_2Cu_3O_{7-\delta}$ sample approaches T_c), the heat flow to the bar Q' will be 4 W. This is physically reasonable. It can be noted that

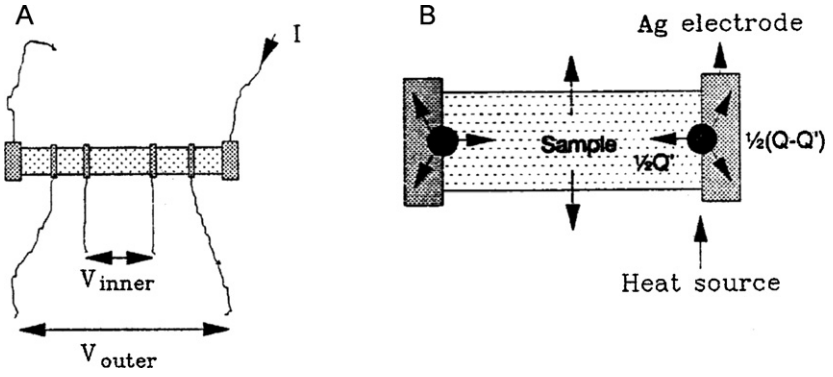

Fig. 5. (A) Six points configuration for J_c measurement, (B) schematic diagram for heat transfer during J_c measurement.

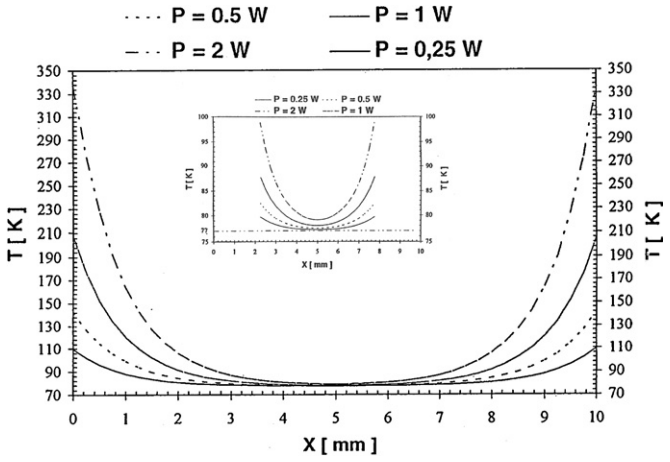

Fig. 6. Calculated temperature profiles along bar of $YBa_2Cu_3O_{7-\delta}$. Calculation parameters bar length = 10 mm, cross section = 1 mm^2, heat transfer coefficient = 1.5 kW m^2 K^{-1}, power dissipation = 0.25 W/contact [11].

samples with poor electrodes (>1 Ω) cracked due to the thermal shock during (J_c) measurement.

This question is resolved by a theoretical thermal model which suggests that a dissipation of maximum 2 W is sufficient to heat a 10 mm bar of $YBa_2Cu_3O_{7-\delta}$ up to T_c [15]. Both this and experiment revealed that the data taken with more than 2 W of dissipation requires caution in the interpretation, Fig. 6.

Secondly, variation in values of (J_c) may occur due to geometry. In this work a criteria of 1 μV cm^{-1} was used to define the critical current. Experiment revealed that for a homogeneous material widening the gap between voltage terminals slightly increased the sensitivity to the transition due to the development of voltage over more material but did not alter the basic (*I–V*) characteristic. It was also necessary not to place the voltage terminals closer than 2 mm to the current terminals, otherwise this can lead to reduced values of (J_c) either due to the thermal effects or a chemical variation of the $YBa_2Cu_3O_{7-\delta}$ in the vicinty of the current terminal.

The most significant effect concerns variation of (J_c) with the cross sectional area transporting the current, Fig. 7. This is generally explained by the generation of a self induced

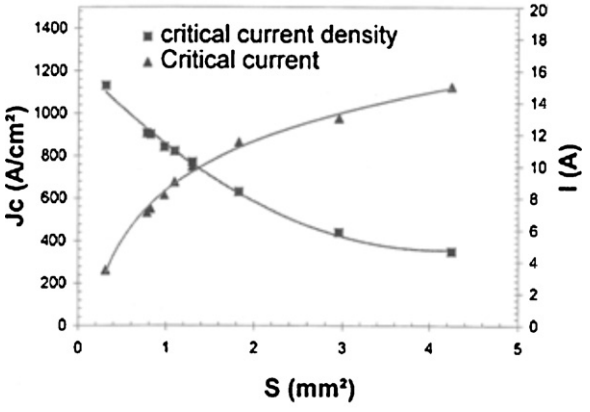

Fig. 7. Current and critical current density measured at 77 K on bars different cross sections.

magnetic field by the flowing current, which limits the critical current density in large cross sectional bars. Following the approach of Dersch and Blatter [26] and [27] concerning a wire in cylindrical form and hallow cylinders, the critical current, (J_c), is related to the material critical current by:

$$\frac{J_c}{J_0} = \left[\frac{A}{R}\right]^{0.5}, \quad \text{with } R > 0.01 \text{ cm} \tag{3}$$

where A is a constant and R is the cylinder radius. Providing R is the maintained constant, the measured J_c values can be compared within a set of samples of different preparations.

3. Results and discussion

3.1. Superconducting state-influence of sintering temperature

This section discusses first the influence of sintering temperature for a given dwell time (yielding strongly different microstructures) on the critical current density to give the mean features. A more detailed discussion is then made of the role of individual factors using the electrical data obtained as a function of dwell time at a chosen sintering temperature. Series of samples were prepared using different starting powders.

An ultrasonic pulse-echo technique was used to evaluate the microstructural state of material. Advantage is taken of the fact that the ultrasonic wave velocity is sensitive to microstructural factors such as microcracks and porosity as well as phase transformation [23]. The evaluation of critical current densities J_c and resistivities at room temperature for sample sintered under different conditions are presented in the Fig. 8. A similar trend for J_c versus sintering temperature with a peak value was also reported by Jin et al. [28]. The first domain of increasing J_c for the samples is characterized by the elimination of porosity and little grain growth. The corresponding decrease in ρ_{300} suggests that the effective current carrying cross section plays the dominant role. The deterioration of J_c for a higher sintering temperature samples sintered under different conditions are presented in Fig. 8A. The densification in the sintering step is virtually complete and there is a strong or even abnormal grain growth. Consequently, microcracks should be present, which will reduce the effective current carrying cross section. However unlike the critical current density the corresponding increase in ρ_{300} is less pronounced, suggesting that the geometrical aspect is not the only factor controlling the electrical properties. Considering that higher temperature sintering involves a liquid phase, second phases (s) may be present in the grain boundary region. Another important factor controlling J_c is the oxygen content. Pores facilitate oxygen access into the sample. Fig. 8C shows the variation of oxygen content and open porosity with sintering temperature. It can be observed that the minimum oxygen content is found where the porosity closes, coinciding with the start of a decrease in J_c. This suggests the oxygen content will be practically constant up to 85% relative density. This knowledge allows the adjustment of sintering conditions to yield a defined microstructure. For example, samples with 85% of theoretical density and small

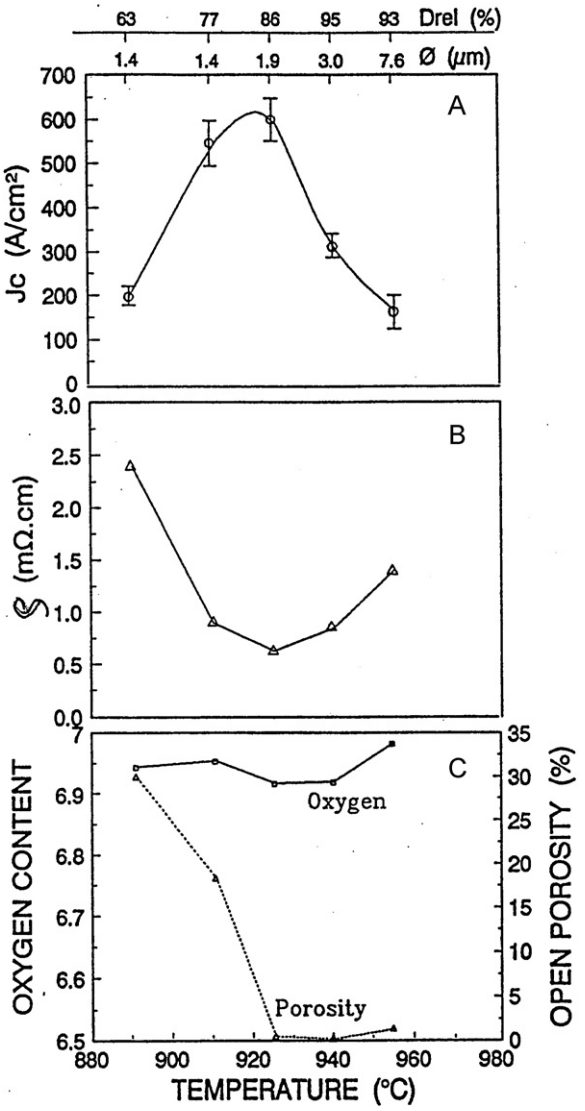

Fig. 8. (A) Critical density at 300 K versus sintering temperature for attrition milled samples (6 h in oxygen). (B) The corresponding resistivity at 300 K. (C) Oxygen content and open porosity.

grain size (2 μm) can be achieved in a reasonable time via the rearrangement and dissolution–reprecipitation stages of liquid phase sintering. Alternatively for denser ceramic, tne coalescence stage can be used to vary the grain size significantly. The final microstructure is also strongly influenced by events during cooling from the sintering temperature. The phase transformation is denoted by a pronounced minimum in Young's modulus. The material then restiffens with oxygen uptake in the orthorhombic phase. Anisotropic volume changes of the unit cell result in stresses which in large grain ceramics are relaxed by microcracking. In practice, samples with an average grain size of 2 μm and 86% of theoretical density are shown to be undamaged.

Finally, the peak value of J_c expresses the compromise between the advantage of greater density and other factors such as poor oxygen content and microcracking. Such a compromise is also evident for a series of samples as a function of sintering temperature, though there is a stronger negative influence of microcracking due to for example, a larger size.

3.2. Porous ceramic-limited grain growth

The role of porosity on the electrical response was explored in more detail using samples sintered at 910 °C and 925 °C for different holding times in oxygen. On cooling the range of relative densities from 68% to 88% of the theoretical value should yield satisfactory oxygenation during the holding at 500 °C for 5 h. This is because the porosity is essentially open and the diffusion path is across one or two grains rather than the sample dimensions. Providing the sintering duration is not longer than 6 h at 925 °C, the grain growth is limited and the average grain size does not exceed 2.5 μm. This means that the stresses on cooling due to the phase transition and below are minimized sufficiently to avoid opening of microcracks. Examination by SEM and TEM, Fig. 1, did not reveal any second phase in samples of this type.

Finally in order to investigate the temperature at which cracks are initiated ($T < 500$ °C) during cooling cycling, cycling between room temperature and 575 °C was performed. This cycling minimized the stresses on the coupling cement while still permitting the microcracking temperature range to be studied. Fig. 9 shows that for 15% porous ceramic with a 2 μm grain size, Young's modulus behaves in a reversible manner with no hysteresis. However hysteresis is observed for 5 μm grain size (15% porosity) and larger. This is the necessary signature where increase in E on heating is due to crack closure and decrease of E on cooling is due to crack opening. Similar behavior has been observed for large grain alumina [29]. The temperature at which the microcracks open (200–300 °C) is lower than that of the maximum oxygen uptake. Though, the

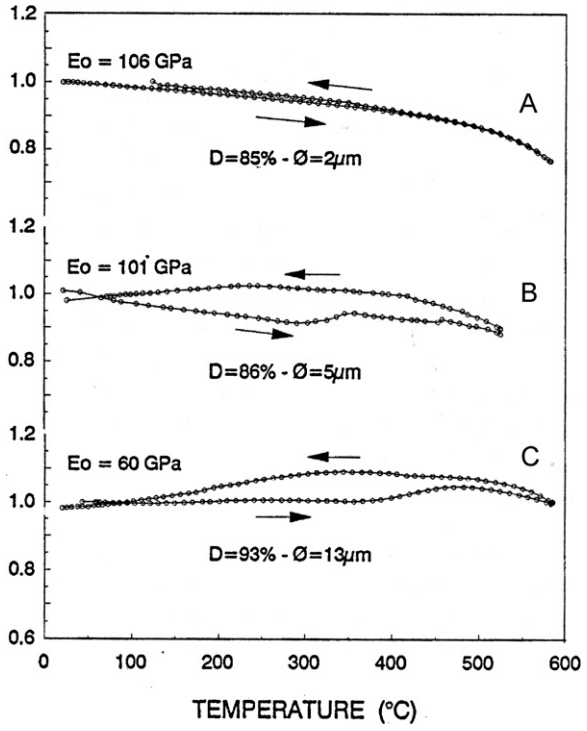

Fig. 9. Young's modulus versus temperature for $YBa_2Cu_3O_{7-\delta}$ showing hysteresis attributed to microcracking. D and Φ represent relative density and average grain size.

oxygen uptake undoubtably plays a role, there is a double action with thermal contraction. In essence during cooling the *b*-axis of the unit cell expands and then contracts acting as a loosening agent for microcracks. The final microstructure is also strongly influenced by events during from the sintering temperature. The phase transformation is denoted by a pronounced minimum in Young's modulus. The material then restiffens with oxygen uptake in the orthorhombic phase. Anisotropic volume changes on the unit cell result in stresses which in large ceramic are relaxed by microcracking. In practice, samples with an average grain size of 2 μm and 86% of theoretical density are shown to be undamaged.

For the attrition milled powder samples sintered at 915 °C in oxygen, no significant grain growth is revealed in the first 12 h of and the examination by SEM and TEM, Fig. 1, did not reveal any second phase in samples of this type. This is supported by the absence of grain growth. The grain growth can be described by a general equation [30]

$$\langle G\rangle^n - \langle G_0\rangle^n = K_0 t \exp\left(\frac{-Q}{RT}\right), \tag{4}$$

where $\langle G\rangle$, $\langle G_0\rangle$ are average grain sizes at time t and $t = 0$, n is an exponent aqual to a value between 1 and 5 depending on the mechanism controlling grain grouth, K_0 is a constant, Q is the apparent activation energy, R is the gas constant and T absolute temperature. Longer duration of sintering time at 925° in oxygen leads to a slow grain growth characterized by an exponent $n = 5$ (the 950 °C data in oxygen for $t < 90$ min also yields this value). Fig. 1C shows a typical microstructure. This reasonably corresponds to the dissolution–reprecipitation stage as suggest by the shrinkage analysis. Such a value has also been found for the ZnO–Bi_2O_3 system, [31], for which it was concluded that the grain growth is controlled by phase boundary reaction. For the $YBa_2Cu_3O_{7-\delta}$ with the liquid phase due to the ternary eutectic, these type of grain growth mechanism my appropriate. Consequently, through the two series of samples variation of porosity should be the predominant effect. Finally for longer sintering time at 950 °C a more rapid grain growth occurs, characterized by an exponent of $n = 2$ in oxygen and 2.5 in air. In addition, the corresponding microstructure shows abnormal growth, Fig. 1D. The previous shrinkage analysis suggests that the coalescence stage has been entered by this time. This means no further shrinkage and significant grain growth, corresponding with the experimental data. The values are in a good agreement with data reported by Shin et al [32]. For their samples sintered at 950–990 °C and $t > 2.5$ h in oxygen yielding $n = 2.1$. Chu et al. [33] found a growth exponent in air $n = 3$, and suggested that grain growth is controlled by diffusion through the liquid layer.

Otherwise, we note from Fig. 4 that the growth though initially impeded, proceeds faster in oxygen. Further evidence for the influence of atmosphere is revealed by the apparent activation energy related to grain growth. Samples were prepared by sintering at different temperature and atmosphere for a fixed dwell time (1.5 h), and grain size was estimated. Using the general growth equation, the estimation of the apparent activation energy, [23] is higher in oxygen, $Q = 188$ kJ/mol compared to air $Q = 126$ kJ/mol. These values are of the same order as those reported by Shin et al. [32].

The influence of porosity on the conductivity can be considered in the context of the two phase problem (KINGERY) [34]. The insulating pore phase affects the combined conductivity in a manner depending on the shape and distribution of the pores. The two extreme cases correspond to either a series or a parallel model. The latter is most relevant to small amounts of porosity and can be described by the relation:

$$\frac{\sigma}{\sigma_0} = (1 - V), \tag{5}$$

where V is the volume fraction of the pore and σ_0 is the conductivity of the solid phase. Fig. 10A and B shows the

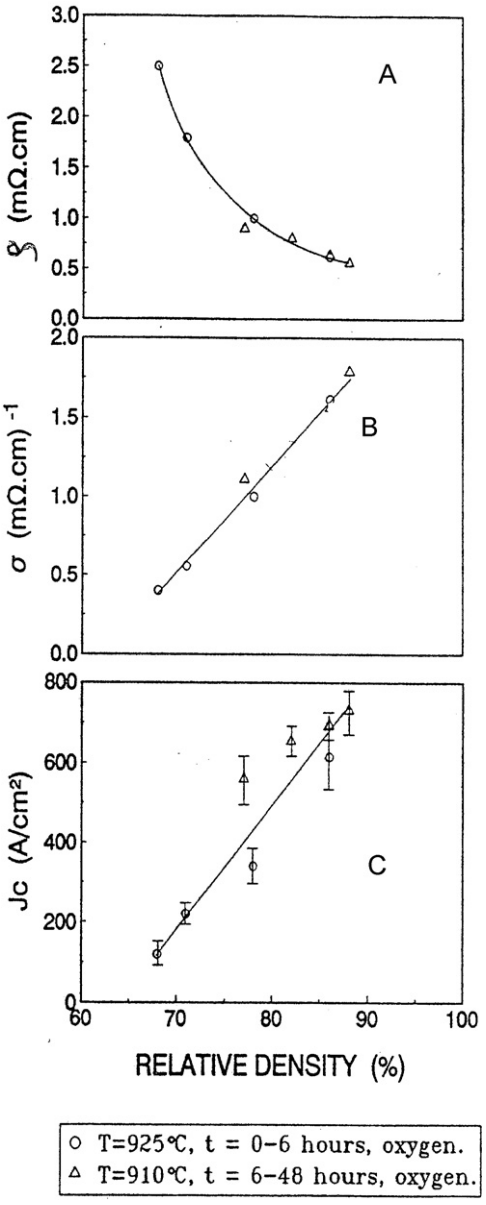

Fig. 10. Electrical properties for $YBa_2Cu_3O_{7-\delta}$ versus relative density of attrition milled samples: (a) resistivity at 300 K; (b) conductivity at 300 K; (c) critical current density at 77 K.

resistivity and the conductivity plotted versus relative density for correlation to critical current density. Typically electrical data for ceramic superconductors in the normal state is presented as resistivity. The resistivity data in Fig. 10A suggests a dependence which is inversely proportional to the relative density consistent with a variation in the effective geometrical factor. This was confirmed by replotting in terms of conductivity (Fig. 10B) giving a linear dependence on relative density similar to other systems such as Zirconia [35]. The same trend can be distinguished in the corresponding critical current data, with greater scatter probably due to measurement problems at high current (Fig. 10C). This suggests that the effective geometrical factor is controlling the electrical response in both normal and superconducting states. An extrapolation of the data yields corrected values for zero porosity of void of 0.4 mΩ cm and 1000 A cm^{-2}. The conductivity representation is preferred since the geometrical cross section then acts on both parameters in the same way) revealing a stronger dependence than the above relation (5). This can be explained by the fact that for these densities the porosity is mostly well connected and, hence, strongly deviates in shape from the ideal model of a spherical pore. A further complicating factor is that $YBa_2Cu_3O_{7-\delta}$ exhibits anisotropic conductivity and ratios between the c-direction and a-b planes ($\rho_c/\rho_{atm.}$) up to almost 100 have been measured on single crystal [21,22]. Using an approach adopted for β_1-alumina, misaligned particles would contribute by increasing the fraction of the insulating phase.

$$\frac{V}{V_0} = 1 + b\frac{(1 - V_0)}{V_0}, \tag{6}$$

where b represents the proportion of misaligned particles. and V_0 is the volume of the solid phase. However, the result of this is a decrease of the dependence of σ on V_0 since:

$$\frac{\sigma}{\sigma_0} = (1 - V_0)(1 - b) \tag{7}$$

A satisfactory conductivity dependence on the pore fraction is consequently difficult due to pore shape and distribution and misalignment and we simply note the approximate linear dependence in a limited range of pore fractions, similar to zirconia [35].

3.3. Denser ceramic-variable grain size

At higher temperatures the duration of the sintering time for a given temperature has two effects: completing the densification and grain growth. The results in this section concern samples which have been slowly cooled in oxygen or reannnealed in oxygen at 500 °C and whose densities situate at this limit.

The competition is less complicated in a series of samples sintered at 950 °C in air and in oxygen. In air which yield approximately constant density, the evaluation of critical current densities J_c resistivity and grain size at room temperature for samples sintered in different conditions are presented in Fig. 11. Grain growth from 4 to 8 μm increases J_c with a parallel decrease in ρ_{300} presumably due to an improved oxygen access via microcracks. Reannealing as a whole

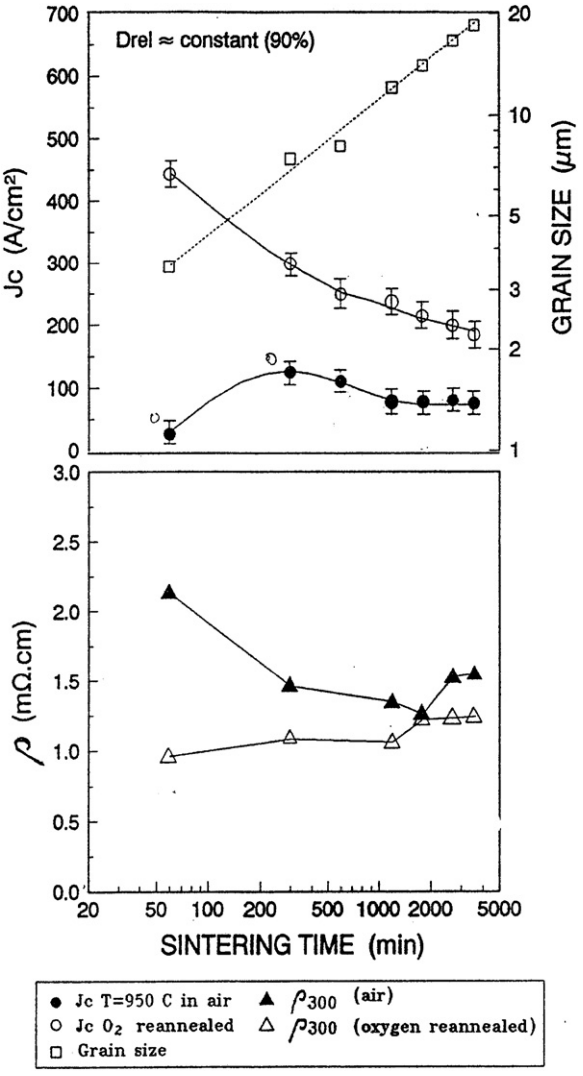

Fig. 11. Critical current at 77 K and resistivity at 300 K versus sintering time for attrition milled samples sintered in air at 950 °C and a rennealed in oxygen.

increases the oxygen content with, as a consequence, increase of microcracking of J_c and decrease of ρ_{300}. The influence of grain growth-induced microcracking is then clearly leading to a steady decrease of J_c (and increase of ρ_{300}). Similar trends with less clarity can be observed in the series of samples sintered at 950 °C in oxygen, Figs. 12.

A similar trend for *Jc* versus sintering temperature with a peak value was also reported in [18]. The first domain of increasing *Jc* for the samples is characterized by the elimination of porosity and little grain growth. The corresponding decrease in ρ_{300} suggests that the effective current carrying cross section plays the dominant role (Fig. 12).

3.4. Relation between the critical current density and the conductivity

The data reported in this paper show a marked correlation between resistivity or even, more clearly, conductivity and the critical current density with respect to trends as the result of altering processing variables. If the current density is plotted

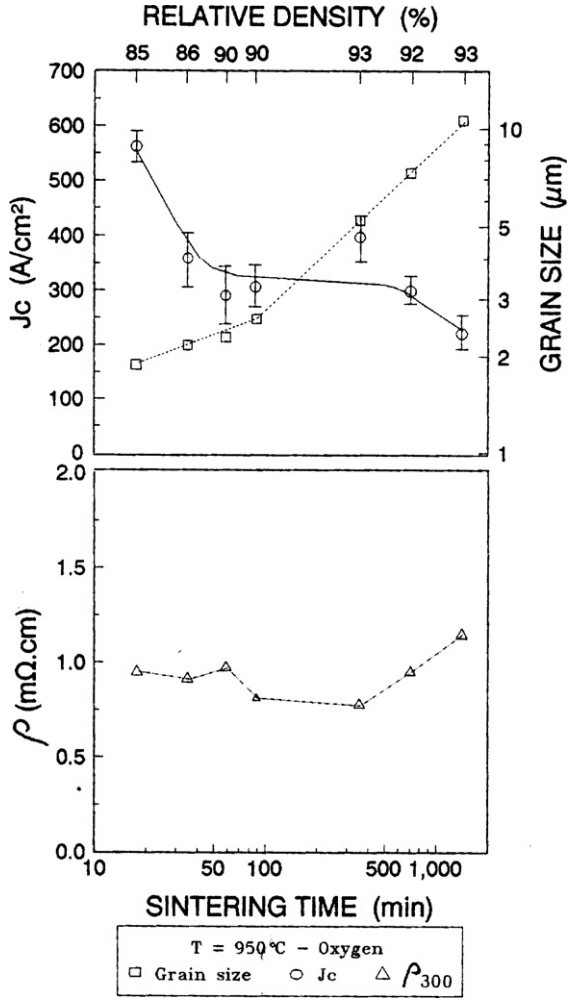

Fig. 12. Critical current at 77 K and resistivity at 300 K versus sintering time for attrition milled samples sintered at 950 °C in oxygen.

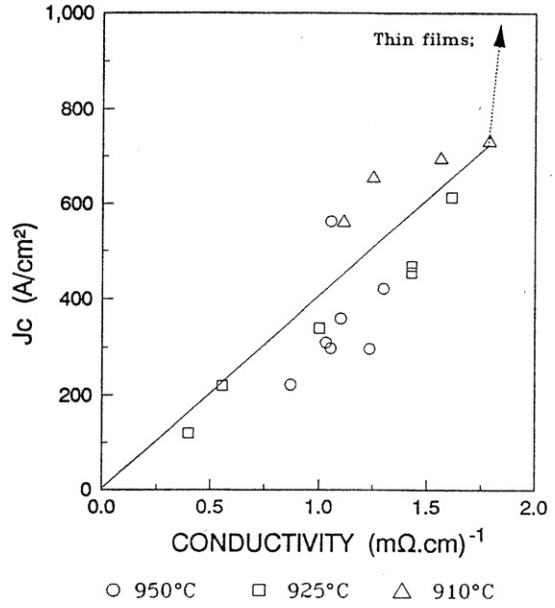

Fig. 13. Critical current at 77 K versus conductivity at 300 K for $YBa_2Cu_3O_{7-\delta}$, sintered in oxygen at different temperature and time.

against conductivity, Fig. 13, a higher value of conductivity corresponds to a higher critical current. Despite some scatter, an almost linear dependence supports the interpretation of the importance of the effective geometrical factor in these data sets. With the elimination of porosity data points climb up the « function» and drop down with microcracking. It would appear that oxygen content, which controls the charge carrier concentration in the normal state, may also yield the same type of correlation. However, since the «function» approaches a limit at zero porosity, other factors must intervene to explain the much larger values of critical current density observed in thin films and single crystals (broken line).

4. Conclusion

The object of the present work was to generate different microstructures for study in relation to the electrical properties. The essential characteristics of a ceramic microstructure are established through densification and grain growth during sintering. However, in $YBa_2Cu_3O_{7-\delta}$. further significant evolution occurs on cooling from the sintering temperature. Consequently, this paper has essentially examined the relation between the preparation, microstructure and electrical properties of bulk ceramic $YBa_2Cu_3O_{7-\delta}$.

The critical current density will depend on the microstructural characteristics: porosity, grain size presence of the second phase in the grain boundary region and oxygen content.

Critical current density and room temperature conductivity show a linear dependence on apparent density related to the effective geometrical factor. However the linear dependence is limited to porous ceramic (densification at 88% of theoretical density) exhibiting small grains (ϕ = 1.5–2.5 μm) and clean grain boundaries. This microstructure provides good oxygen access and avoids microcracking.

In contrast, for larger grained ceramic, the presence of microcracks was confirmed by ultrasonic measurements. Microcracks facilitate oxygen access, but reduce the effective current carrying cross section resulting in a decrease of critical current density.

Porosity and microcracks have a direct influence on the effective current carrying cross section. Their presence will decrease the critical current density and increase resistivity. Second phase in the grain boundary region may also intervene to decrease J_c and ideally should be avoided. Oxygen content also has a direct role for J_c and resistivity. However oxygen access becomes in dense ceramic. In larger grain material, microcracks provide an alternative path but this is not a desirable solution.

In practice, highest J_c values can be achieved on samples with small grains (2 μm) and which are relatively porous (86% of theoretical density). This microstructure, on cooling relaxes the stress without microcracks and promotes oxygen uptake. Furthermore sintering at low temperature (915–925 °C) is preferable in order to obtain clean grain boundary.

In order to adopt the orthorhombic phase, $YBa_2Cu_3O_{7-\delta}$ takes up oxygen on cooling. The carrier concentration depends on the oxygen content and this can be seen by a dependence of the normal state resistivity. Though almost all preparation

procedures seek to maximize the oxygen content by annealing at 400–500 °C, this parameter is sensitive to the microstructure defined in the sintering step.

To obtain a high critical current density for bulk ceramic $YBa_2Cu_3O_{7-\delta}$, the following conditions must be met:

- full oxygenation
- absence of cracks
- clean grain boundaries.

These conditions can be achieved in porous ceramic with a relative density of ≈88% of the value for theoretical density with a small grain size ($\phi \approx 2\ \mu m$)

An alternative strategy for large grain ceramics can be carried out by mechanical means. However due to the necessarily high temperature processing, copper rich second phase is frequently observed. Furthermore the incomplete alignment of grains in the center of the sintered samples (hence microcracking) requires further study.

The physics of the system must take into account: alignment of grains, grain boundaries, porosity, microcracks, and sample geometry. A first approach to polycrystalline ceramic assumes random grain orientations and though the pressing step may induce a slight texturation, the working assumption for the samples in this work is random orientations.

References

[1] J.G. Bernorz, K.A. Muller, Z. Phys. 64 (1986) 189.
[2] M.K. Wu, J.R. Ashbwn, C.J. Torring, P.H. Hor, R.L. Merg, L. Gao, Z.J. Hunag, Y.Q. Wong, C.W. Chu, Phys. Rev. Lett. 58th (9) (1987) 908.
[3] N.McN. Alford, W.J. clegg, M.A. Harmer, J.D. Birchall, K. Kendall, D.H. Jones, Nature 332 (1988) 58–59.
[4] J.W. Ekin, Adv. Ceram. Mater. 2 (3b) (1988) 595.
[5] X.G. Zhang, H. kurigaki, K. Hiraltawa, Supercond. Sci. Technol. 3 (39) (1990) 334.
[6] E.M. Gyorgy, G.S. Grader, D.W. Johnson Jr., L.C. Feldman, W.W. Rhodes, R.E. Hazard, M.P. Manlliewich, W.J. Skoopol, Appl. Phys. Lett. 52 (4) (1988) 328.
[7] S. Jin, T.H. Tiefel, R.C. Sherwood, R.B. Van Dover, M.E. Davis, G.W. Kammlott, R.A. fastnacht, O.F. Lima, Phys. Rev. B 37 (13) (1987) 7850.
[8] K. Watamaka, N. Katawasky, H. Yamane, T. Hirai, Y. Muto, H.T.S. Kawaba, in: C. Freyhardt, R. Flukiger, M. Peuckeurt (Eds.), Materials Aspects, 965, Deutsche Gesellchaft fur Material Runde, 1991, p. 870.
[9] J.E. Tkazzyk, C.C. Brrant, J.A. Delmant, F.L. Hall, P.L. Karas, K.W. Lay, E. Narumia, D.T. Shaw, J. Mater. Res. 7 (1992), 1817-1327.
[10] W.H. Chu, N. Zhu, L. Tan, S. Serigupta, P.J. McConn, Abstracts of the American Ceramic Society Meeting, Cieneinati, 1991.
[11] M.P. Siegal, S.Y. Han, J.M. Phillips, T.H. Tieffal, J.H. Marshall, J. Mater. Res. 7 (1989) 2658.
[12] E. Cazy, A. Khalfi, D.S. Smith, J.P. Bonnet, J. Mater. Res. 12 (6) (1997) 1451–1455.
[13] A. khalfi, D. Smith, B. Soulestin, G. Trolliard, P. Marchet, J.P. Bonnet, P. Odier, F. Gotor, J. Mater. Sci. Lett. 18 (octobre 1999) 1575–1577.
[14] C.A. D'Ovidio, J.E. Fiscina, D.A. Esparza, J. Appl. Phys. 69 (1991) 8265–8267.
[15] D. Smith, A. Khalfi, N. Ghayoub, E. Cazy, J.P. Bonnet, A.E. Abraham, Physica C 281 (1997) 76–84.
[16] S. Suasmoro, D. Smith, M. Lejeune, European Ceramic Society Meeting, vol. 18, 1992, pp. 91–97.
[17] E. Cazy, A. Khalfi, D. Smith, M. Huger, J.P. Bonnet, J. Mater. Sci. 42 (August (15)) (2007) 6310–6315.
[18] J.G. Thompson, B.G. Hyde, R.L. Withers, J.S. Anderson, Mater. Res. Bull. 22 (1987) 1715–1724.
[19] H.S. Harowitz, R.K. bordia, R.B. Flipper, R.E. Johnson, U. Chwdhry, Mater. Res. Bull. 20 (1988) 821–830.
[20] E. Cazy, D. Bahloul, D. Smith, J.P. Bonnet, J. Phys. III (Paris) 4 (1994) 2105.
[21] D.S. Smith, S. Suasmoro, C. Gault, J. Eur. Ceram. (1992) 81–85.
[22] S. Susmoro, D. Smith, M. Lejeune, M. Huger, C. Gault, J. Mater. Res. 7 (1992) 1629–1635.
[23] S. Suasmoro, Elaboration de céramiqes massives $YBa_2Cu_3O_{7-\delta}$—evolution. microstructurale et propriétés électriques, Doctorat de l'université de Limoges, soutenue le 7 Mai 1992.
[24] N. Chen, D. Shi, K.C. Goretta, J. Appl. Phys. 66 (6) (1989) 2485.
[25] M.I. Mendelson, J. Am. Ceram. Soc. 52 (8) (1969) 443;
L.W. Hobbs, J. Am. Ceram. Soc. (1981).
[26] H. Dersch, G. Blatter, Phys. Rev. B 38 (1988) 11391–11404.
[27] D. Smith, A. Khalfi, T. Chartier, E. Ebraham, Physica C 350 (2001) 37–45.
[28] S. Jin, R.C. Sherwood, T.H. Tiefel, R.B. Van Dover, G.W. Kammlott, M.E. Davis, R.A. Fastnacht, S. Nakahara, M.F. Yann, D.W. Johnson Jr., Mater. Res. Soc. Proc. 99 (1988) 773.
[29] E.D. Case, J.R. Smyth, O. Hunter, J. R. Mater. Sci. Eng. 51 (1981) 175.
[30] R.J. Brook, in: F.F.Y. Wang (Ed.), Treatise on materials science and technology, vol. 9, Ceramics Fabrication Process, 1976, p. 331.
[31] T. Senda, R.C. Brandt, J. Am. Ceram. Soc. 73 (1) (1990) 106.
[32] M.W. Shin, T.M. Hare, A.I. Kingon, C.C. Koch, J. Mater. Res. 6 (10) (1991) 2026.
[33] C.T. Chu, B. Dunn, J. Mater. Res. 5 (9) (1990) 443.
[34] W.D. Kingery, E. Niki, M.D. Narasimhan, J. Am. Ceram. Soc. 44 (1) (1961) 29.
[35] M. Kleitz, H. Bernard, E. Fernandez, E. Schouler, Advances in Ceramic, vol. 3, Science and Technology of Zirconia, 1981, pp. 310–336.